

Separable Representations for Duration and Distance in Virtual Movements

Keri Anne Gladhill¹, Eva Marie Robinson², Candice Stanfield-Wiswell¹, Farah Bader¹, and Martin Wiener¹

Abstract

■ To navigate through the environment, humans must be able to measure both the distance traveled in space, and the interval elapsed in time. Yet, how the brain holds both of these metrics simultaneously is less well known. One possibility is that participants measure how far and how long they have traveled relative to a known reference point. To measure this, we had human participants (n = 24) perform a distance estimation task in a virtual environment in which they were cued to attend to either the spatial or temporal interval traveled while responses were measured with multiband fMRI. We observed that both dimensions evoked similar frontoparietal networks, yet with a

striking rostrocaudal dissociation between temporal and spatial estimation. Multivariate classifiers trained on each dimension were further able to predict the temporal or spatial interval traveled, with centers of activation within the SMA and retrosplenial cortex for time and space, respectively. Furthermore, a crossclassification approach revealed the right supramarginal gyrus and occipital place area as regions capable of decoding the general magnitude of the traveled distance. Altogether, our findings suggest the brain uses separate systems for tracking spatial and temporal distances, which are combined together along with dimension-nonspecific estimates.

INTRODUCTION

The perception and production of both temporal and spatial features of the environment is necessary for mobile organisms to interact with and navigate through the world. However, it is not yet fully understood whether these dimensions rely on shared or differential neural circuits (Robinson, Michaelis, Thompson, & Wiener, 2019; Marcos & Genovesio, 2017; Martin, Wiener, and & Wassenhove, 2017; Cai & Connell, 2016; Bueti & Walsh, 2009). These divergent findings could be because of the natural correlation of both temporal and spatial magnitudes, in that longer distances typically take more time to traverse, making it difficult for humans to attend to spatial information without also taking into account temporal information (Riemer, 2015). In fact, brain areas such as the pFC and right parietal cortex have been implicated in different types of magnitude processing, specifically those of time and space (Bueti & Walsh, 2009). Other studies suggest a neural dissociation between temporal and spatial processing; specifically, spatial tasks activate more posterior regions such as the parahippocampal gyrus, anterior hippocampus, and retrosplenial cortex (RSC; Cona & Scarpazza, 2019; Peer, Ron, Monsa, & Arzy, 2019; Kim & Maguire, 2018; Gauthier & van Wassenhove, 2016), whereas temporal tasks exclusively activate the SMA (Coull, Charras, Donadieu, Droit-Volet, & Vidal, 2015). Yet, a recent meta-analysis of neuroimaging studies of time and space revealed a rostrocaudal gradient of activation-likelihood in the SMA for space and time, suggesting that spatiotemporal contingencies are processed in a hierarchical manner (Cona, Wiener, & Scarpazza, 2021), with space serving as a "scaffold" through which time can be processed. Additional gradients were also observed in the right inferior parietal lobe (IPL) and right pFC, suggesting these regions also mediate perceptual responses for temporal and spatial dimensions.

More recent studies have demonstrated the ability to separate time and space from one another by using virtual reality (VR) environments (Bansal, Weech, & Barnett-Cowan, 2019; Robinson et al., 2019; Thurley & Schild, 2018; Deuker, Bellmund, Navarro, & Doeller, 2016; Wiener, Michaelis, & Thompson, 2016; Petzschner & Glasauer, 2011). Specifically, VR environments allow spatiotemporal contingencies to be separately manipulated (Bansal et al., 2019), such that long distances can be reached in short periods, and vice versa, allowing researchers to observe dissociable impacts of each dimension on perception and choice. Yet, the brain networks underlying these computations have not yet been measured: Do time and space share processing across a gradient, or do they rely on separate, parallel channels?

Recent work on this topic has provided mixed evidence. Using EEG, we have shown that electrophysiological signatures for measurements of time and distance are dissociable, with time employing a "preplanning" strategy for navigating in time, and space employing a landmark strategy (Robinson & Wiener, 2021). The preplanning strategy

¹George Mason University, Fairfax, VA, ²University of Arizona

involves setting the speed of an internal timer until a fixed threshold is reached, whereas the landmark strategy involves selecting a target location and moving until that position is reached. Yet, both require participants to establish a "starting point" when moving through an environment. Notably, both strategies were evident in indices putatively driven by the SMA. However, another work has shown that time and distance rely on separable neural networks, with interactions dependent on the direction of influence; distance effects on time are mediated via motion-sensitive visual regions, whereas the influence of time on distance perception comes via extrastriate sensory integration regions of the parietal lobe (Riemer, Achtzehn, Kuehn, & Wolbers, 2022).

To dissociate the influence of time and space on one another and thereby examine dissociable brain networks, we measured fMRI while human participants integrated distance or time in a VR environment. Analytically, we used a multivariate decoding method to characterize neural regions containing time or distance-sensitive patterns of activity, as well as a cross-classification method to measure dimension-nonspecific representations of either dimension. Critically, we discouraged participants from using the non-attended dimension to aid in reproducing the attended one to avoid cross-modal influence, assuring that any dimension-nonspecific regions were not because of natural spatiotemporal correlations. Our findings confirm a rostrocaudal gradient for space and time, revealing both specialized regions for each dimension as well as dimension-nonspecific regions associated with general signal magnitude.

METHODS

Participants

This study included 23 right-handed participants that were neurologically and psychiatrically healthy (15 female, 7 male, 1 undisclosed; 18–29 years old, M = 22.2) recruited at George Mason University. The sample size for this study was based on previous work from our laboratory using this design (Robinson & Wiener, 2021; Wiener et al., 2016). All participants satisfied the MRI safety screening criteria and provided consent as approved by the university institutional review board at George Mason University. Participants were compensated for their time with monetary payment. Because of a software error during data collection, we note that seven participants did not have their behavioral data saved; as such, all behavioral and multivariate decoding analyses are conducted on the remaining 16 participants, and the univariate analyses are reported on the full 23 participants.

Task

Participants completed temporal and spatial reproduction tasks in a virtual environment (VE) while undergoing fMRI

using a SIEMENS Prisma 3 T scanner with a 32-channel head coil. The VE was previously used in behavioral (Robinson et al., 2019) and EEG (Robinson & Wiener, 2021) studies from our laboratory (Figure 1). The paradigm was originally developed by Petzschner and Glasauer (2011) and designed using Vizard 5.0 (Worldviz), a Python-based software. The ground in the VE was created using a black-and-white noise image that resembled a textured "desert" ground. There were 20 identical scattered rocks imported from SketchUp 3-D (Trimble Navigation) and a sun, in the form of a sphere on the horizon. The clear sky was a simulated 3-D dome included in the Vizard software. Importantly, the construction of the VE minimized reliable environmental distance cues by randomizing the initial viewpoint and position/orientation of each rock at the start of each trial. In addition, the 3-D sky made it appear as though the horizon was always a constant distance away. Participants completed the task by viewing the VE through a head coil mounted mirror that reflected the monitor (Cambridge Research Systems Display++, 120-Hz refresh rate) at the end of the scanner's bore during scanning and respond using an MR-compatible handheld button box (Current Designs) with four buttons aligned horizontally (only furthest left and right buttons used).

Procedure

Trials were completed in blocks of 14 trials per block, for eight blocks, each lasting approximately 6 min. TIME trials and DISTANCE trials were presented randomly within each block, consisting of seven possible trials of each type. Each trial consisted of an estimation and reproduction phase. The estimation phase began after a white fixation cross on a black background for a variable interval drawn from an exponential distribution with a minimum duration of 3 sec (Wiener et al., 2016); above the fixation cross, participants viewed the words "Estimate Time" or "Estimate Distance." Participants began with a random view of the horizon in the VE and a red sphere appearing on the horizon. Participants pressed the left button to begin movement toward the red sphere. After a particular distance (DISTANCE trials) or temporal interval (TIME trials) had passed, movement was automatically stopped, the red sphere disappeared, the screen dimmed, and the words "REPRODUCE DISTANCE/TIME" appeared. Following a variable 4- to 8-sec delay (uniform distribution), the words disappeared, the screen re-illuminated, and the reproduction phase began. The reproduction phase began the same as the estimation phase (left button press to begin movement) and participants reproduced the distance or time traveled in the estimation phase by terminating the movement with a right button press. As a reminder, the appropriate magnitude was displayed in the upper left corner (e.g., the word "TIME" was displayed on time trials) to ensure that participants did not forget the dimension to be reproduced (Thurley & Schild, 2018). The sphere on the

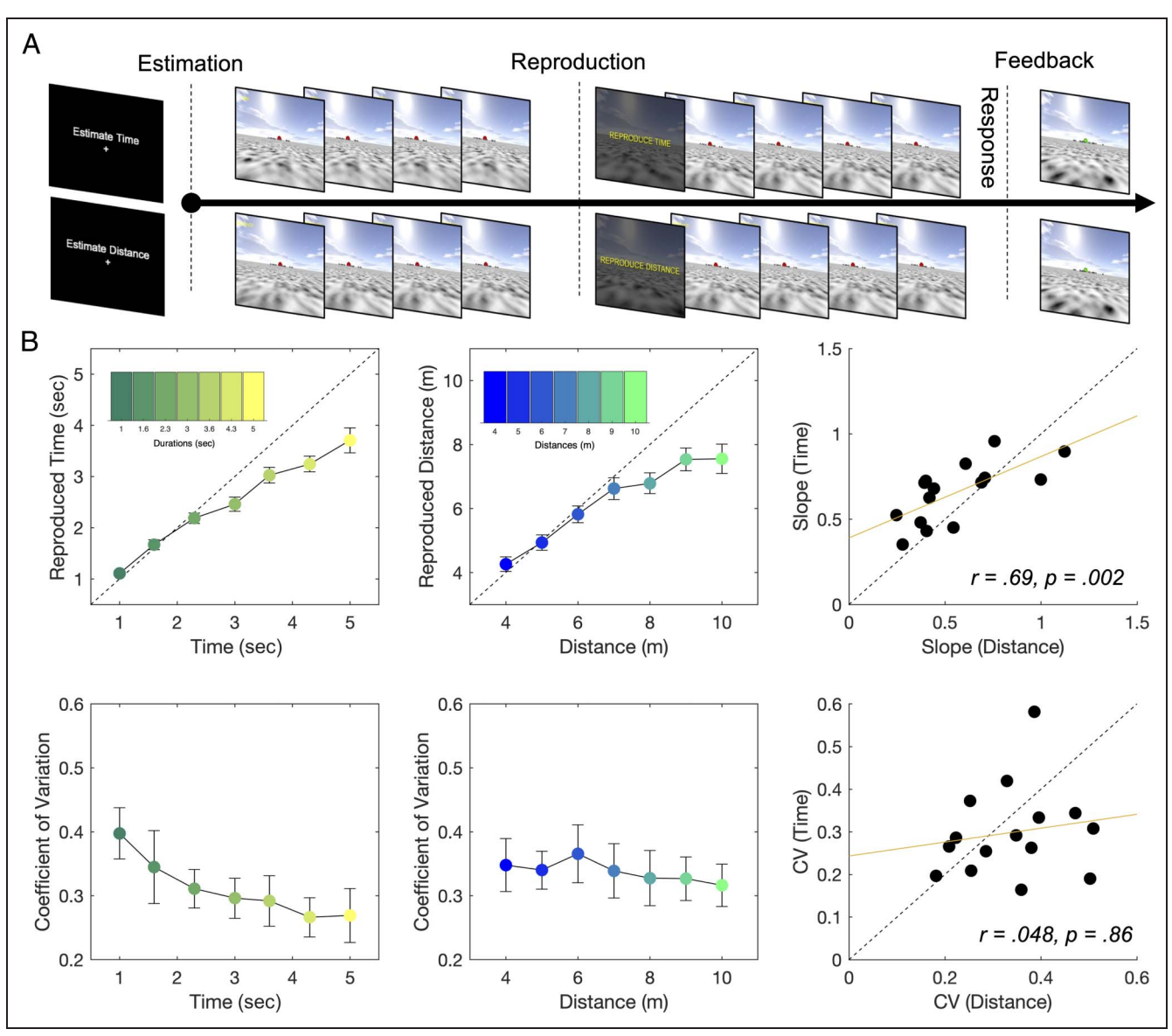


Figure 1. Task and behavioral data. (A) Participants performed a distance reproduction task within a VR environment. On a given trial, participants were initially prompted to estimate either time or distance, after which they were placed at a random point in an open field environment facing a distant red sphere. Participants moved forward while estimating the relevant dimension, after which they were told to reproduce that same dimension. Walking speed varied between estimation and reproduction phases. Feedback was provided after participants made their response. (B) Reproduced times and distances as a function of target intervals are displayed (mean \pm *SE*); participants exhibited gradual underreproduction of both dimensions with longer intervals. The right column displays slope values for both dimensions, which were significantly correlated; furthermore, participants exhibited higher slope values for distance reproduction, indicating more accurate performance. Bottom columns display normalized variability (coefficient of variation; CV) for both dimensions for each interval tested. Bottom right column displays CV values collapsed across interval; no difference or correlation was detected.

horizon provided feedback by re-appearing as green if reproduction was accurate or red if it was inaccurate. The feedback was adaptive on a trial-by-trial basis such that the feedback constant (k) was updated in a 1-up/1-down rule (step size = .015) if the reproduced interval was within (step-down) or outside of (step-up) the feedback window (interval/k). Starting k value was 3.5 (Robinson & Wiener, 2021; Jazayeri & Shadlen, 2010) and was calculated separately for time and distance; in this way, positive feedback was received if the trialwise reproduction values fell within a window of possible intervals that adjusted

itself based on previous responses. The distances used in the estimation phase of DISTANCE trials was randomly selected from seven linearly spaced intervals between 4 and 10 m. On the estimation phase of TIME trials, the distance was determined by the temporal interval and varied across seven linearly spaced intervals between 1 and 5 sec. The speed of movement was drawn randomly from a uniform distribution between 2 and 4.5 m/sec to match the duration experienced on spatial reproduction trials to those presented in temporal reproduction trials, while also matching the distances used on temporal

reproduction trials to those experienced on spatial reproduction trials (Robinson & Wiener, 2021). In addition, to eliminate the possibility of participants using the time spent moving as a measure of distance or the distance walked as a measure of time traveled, the simulated walking speed was randomly altered between estimation and reproduction phases such that it was noticeably faster or slower than the estimation phase speed (maximum +60% estimation speed, drawn from a normal distribution). Participants were instructed not to count or tap during the task (Rattat & Droit-Volet, 2012) and were not aware of the range of distances or times but were aware that the walking speed was altered.

fMRI

Scanning was conducted using a 3 T Siemens Prisma Magnetom scanner. All participants initially received a high-resolution, T1-weighted, 3-D magnetization prepared rapid gradient echo scan (192 coronal slices, repetition time [TR] = 2400 msec, echo time [TE] = 2.28 msec, inversion time = 1060 msec, matrix size 300×320 , .8-mm isotropic voxels). Following this, a gradient echo fieldmap was collected (64 coronal slices, TR = 1200 msec, TE = 33 msec, matrix size = 84×84 , voxel size = 2.5-mm isotropic voxels). Multiband gradient-EPI were individually acquired (64 coronal slices, TR = 1200 msec, TE = 33 msec, matrix size 84×84 , voxel size = 2.5-mm isotropic voxels). EPI volumes were acquired in eight separate runs, with each run lasting a variable duration (~6 min). The first three volumes of each run were additionally discarded to allow for steady-state magnetization.

Behavioral Analysis

Behavioral data were analyzed similar to our previous report (Robinson & Wiener, 2021). Briefly, the mean reproduced duration and distance were calculated for each participant and interval tested. In addition, the coefficient of variation (standard deviation/mean) was calculated as a measure of variability. To further quantify performance, we fit mean reproductions with a simple linear regression and calculated the slope values for each dimension; a slope value closer to zero indicates a larger central tendency effect, wherein responses gravitate to the mean, whereas a value closer to one indicates more veridical performance.

fMRI Analysis

Analysis of fMRI images was conducted using SPM12 (https://www.fil.ion.ucl.ac.uk/spm/). Standard preprocessing steps were conducted for each participant, including realignment, normalization, and smoothing (6 mm). In addition, before realignment, we corrected for fieldmap homogeneity using Hyperelastic Susceptibility Artifact Correction (Ruthotto et al., 2012) module in the Artifact Correction in Diffusion MRI (ACID) toolbox for SPM. At

the first level (single-subject), a general linear model was constructed by convolving the onset times of events with a canonical hemodynamic response function. More specifically, we specified events at the onset of either the estimation phase or the reproduction phase of time and distance trials, separately. In addition, we modeled the hemodynamic response function with a boxcar function, to account for the varying durations of each interval (Wiener et al., 2016). At the second-level (group), we conducted several planned contrasts, including (Time Reproduction > Time Estimation), (Distance Reproduction > Distance Estimation), and (Time Reproduction – Distance Reproduction). Note that the final contrast was examined in both directions. For this and all other comparisons, significance was set at a voxel level threshold of p < .001 and a cluster-level threshold of p < .05, FWE corrected. Anatomical localization was conducted using the SPM Anatomy Toolbox. To further interrogate activity within the RSC, we defined a functional map using the Neurosynth database (www .neurosynth.org) with the search term "RSC"; a forward inference z-map was extracted and thresholded at z =2.5 to include only voxels within the precuneus region, behind the posterior commissure (Chrastil, 2018). This map was converted into a binary mask that was used in all analyses with a small volume correction. That is, a whole-brain analysis was conducted using the significance threshold described above, except within the RSC region. We specifically used the RSC as a ROI for this analysis on the basis of our previous finding for this region in this exact task (Wiener et al., 2016). Our reasoning for using a mask for the RSC, specifically, is because of the difficulty in defining this region; indeed, the RSC is not included in general anatomical atlases, but rather is defined on a probabilistic basis from anatomical and functional data (Chrastil, 2018). As such, prior studies have defined the RSC using a priori methods, as employed here.

Multivariate decoding was performed using The Decoding Toolbox (Hebart, Görgen, & Haynes, 2015). To perform this, we used functional data from the step before smoothing, to maintain more granular activation patterns. A new first-level general linear model was constructed, with separate regressors for each interval of time and distance tested. These resulting beta maps were subjected to a whole-brain searchlight analysis (6-mm searchlight) in which, at each location, a support vector machine was trained and tested in a leave-one-run-out, cross-validation procedure on the seven intervals tested for each dimension. Separate decoding analyses were conducted for time and distance, at both the estimation and reproduction phases, resulting in (accuracy-chance) maps for each condition. These maps were then smoothed as for the univariate analysis with a 6-mm Gaussian and then combined for a group-level analysis using one-sample t tests with the same significance threshold as above. Cross-classification analysis was conducting using the make design xclass function from The Decoding Toolbox, in which the classifier was trained using the intervals of one dimension and then tested on intervals from the other dimension, again in a leave-one-run-out cross-validation procedure.

RESULTS

Similar to previous reports, we observed that participants exhibited a central tendency effect, in which reproduced estimates gravitated to the mean of the stimulus set. We additionally note that this effect was offset from the true mean of the stimulus set for each dimension, such that participants gradually underreproduced both time and distance with larger values (Riemer & Wolbers, 2020; Eisler, 1976). Notably, this effect was larger for time than for distance, t(15) = -3.078, p = .008, Cohen's d = .769, and was also correlated between dimensions (r = .7, p =.003), suggesting a common mechanism for reproducing magnitudes (Martin et al., 2017). In contrast, when examining the variability of reproduced estimates, we observed no difference between time and distance, F(1, 15) = .467, p = .505, nor any interaction with the tested interval, F(6, 90) = 1.156, p = .337, and no correlation between the two (r = .048, p = .86; Figure 1).

Time and Distance Reproduction Activate Overlapping Networks

In our scanning protocol, we initially performed a univariate analysis of BOLD activation while participants performed the task. Previously, using the distance version of this task, we observed that the reproduction phase activates a bilateral frontoparietal network of regions, as well as subcortical sites across the basal ganglia and hippocampus (Wiener et al., 2016). Our findings here replicate this effect, with distance reproduction activating a broad network of brain regions across the basal ganglia, cerebellum, ACC, right pFC, and parietal and occipital regions, as well as the right hippocampus (Figure 2, Table 1). Notably, time reproduction activated a similar network of regions, although without any activation in the hippocampus (Figure 2, Table 2). In contrasting these effects against one another, we observed a striking dissociation between dimensions across the central sulcus; distance reproduction preferentially activated a variety of posterior regions, including a cluster of regions extending from the middle occipital gyri to the inferior parietal lobes and from the thalamus to the cerebellum, including the bilateral hippocampus (Figure 2, Table 3). In contrast, time reproduction exclusively activated a single region in anterior cortex—the bilateral SMA (Figure 2, Table 3). These findings suggest a division of labor between rostral and caudal parts of the brain in coordinating movements for distance and time.

Time and Distance Can Be Decoded during Reproduction

To further examine distance and time estimates in the brain, we employed a multivariate decoding technique,

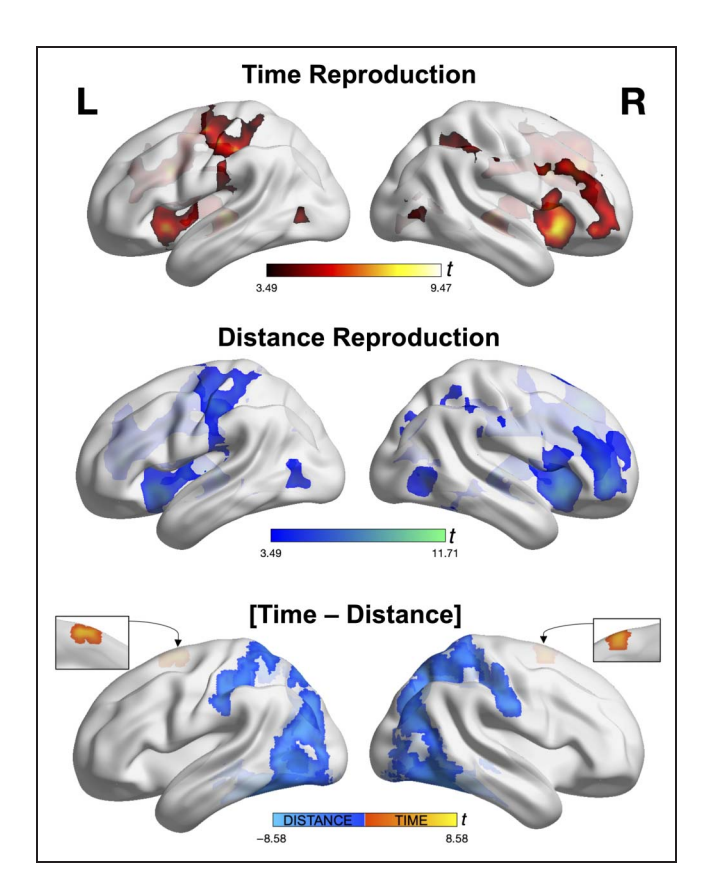


Figure 2. Univariate fMRI results for time and distance reproduction. The top displays significant activation when participants reproduced time estimates. Clusters of activation were observed in frontoparietal structures, including inferior frontal gyrus, inferior parietal lobe, SMA, basal ganglia, and cerebellum (not shown). The middle displays significant activation when participants reproduced distance estimates. Clusters of activation were again found in similar frontoparietal regions, as well as subcortical regions including basal ganglia, cerebellum, and also hippocampus. Both time and distance contrasts were from comparing reproduction phase activity against estimation phase activity. The bottom displays the contrast of time with distance reproduction. Here, distance reproduction preferentially activated posterior regions across striate and extrastriate cortex, as well as bilateral parietal regions and the hippocampus. In contrast, time reproduction only activated the SMA bilaterally. All clusters thresholded at height p < .001 uncorrected and cluster p < .05FWE error corrected.

in which a whole-brain searchlight (6 mm) was used to train a support vector machine on intervals of time and distance. During the reproduction phase, we again observed a dissociation between decoding accuracy across two distinct regions. For time, significant decoding accuracy was observed in the SMA, precentral gyrus, and inferior frontal gyri. For distance, in contrast, we observed significant accuracy in several areas, including the left caudate and cerebellum, yet the only region to survive our significance threshold was the RSC (Figure 3, Table 4). One point of connection between decoding accuracy and behavioral performance is the possibility that the fidelity with which we could decode either dimension (duration or distance)

Table 1. Univariate Activation for Time Reproduction

Location	Cluster Size	t Value	x	y	z
L thalamus	6207	9.475	-2	-25	3
R insula lobe		8.468	31	18	-3
L caudate nucleus		8.377	-10	8	-3
L ACC	5354	8.613	-7	13	33
L precentral gyrus		7.892	-37	-10	55
R ACC		7.845	6	31	28
R cerebellum (VI)	2557	7.864	21	-52	-25
R cerebellum (VIII)		7.456	13	-67	-45
L cerebellum (Crus 1)		6.415	-37	-55	-35
L middle temporal gyrus	236	6.206	-42	-67	0
L middle occipital gyrus		4.227	-35	-80	15
R inferior parietal lobule	798	5.569	43	-50	53
R superior parietal lobule		5.209	31	-37	40
R postcentral gyrus		4.676	56	-20	35
R inferior occipital gyrus	165	5.261	41	-62	3
R precuneus	112	4.733	16	-65	40

Table 2. Univariate Activation for Distance Reproduction

Location	Cluster Size	t Value	x	у	z
L caudate nucleus	21972	11.711	-10	11	-5
R caudate nucleus		10.356	11	8	-5
R ACC		10.066	8	38	18
R middle temporal gyrus	337	5.656	48	-70	5
L inferior occipital gyrus	340	5.487	-42	-70	0
L superior occipital gyrus	141	4.697	-22	-77	30
L middle occipital gyrus		4.528	-32	-82	13

 Table 3. Univariate Activation for Comparisons between Time and Distance Reproduction

Region Label	Extent	t Value	x	y	z
[Distance – Time]					
R fusiform gyrus	9717	8.583	36	-42	-13
L fusiform gyrus		7.351	-35	-52	-13
L middle occipital gyrus		7.339	-32	-72	28
R thalamus	317	7.162	23	-27	13
R thalamus		4.598	8	-15	3
L cerebellum (IX)	196	5.274	-15	-50	-53
L cerebellum (X)		3.943	-22	-32	-43
[Time – Distance]					
L SMA	151	6.424	-5	1	65

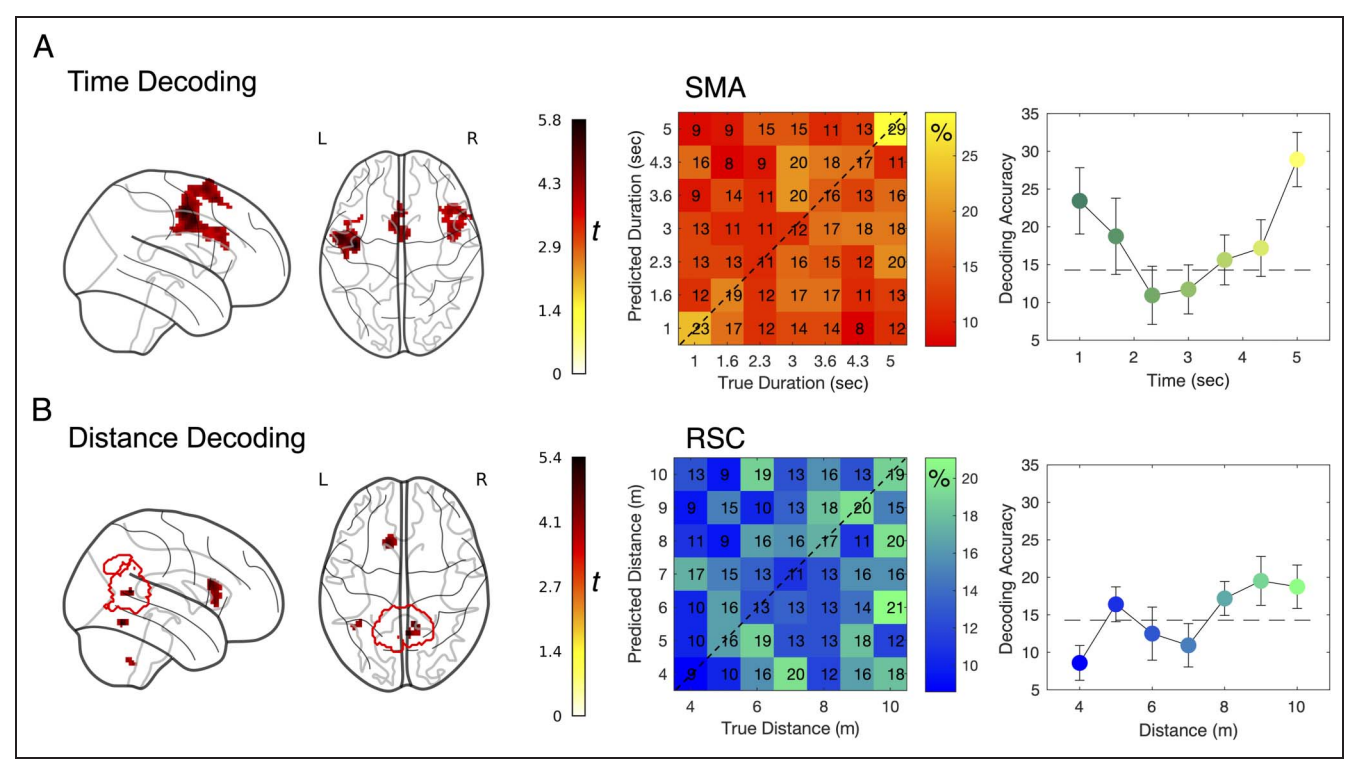


Figure 3. Decoding of time and distance estimates. (A) Decoding of time estimates during time reproduction revealed activation within the SMA, precentral gyrus and inferior frontal gyri (left columns). The middle column displays the average confusion matrix for this region, containing the average percentages, across participants, of predicted durations against the true duration label; note that the rows of predicted durations sum to 100%, as they pertain to the proportion of guesses for each possible interval by the classifier. (B) Decoding of distance estimates during distance reproduction revealed significant decoding in several clusters, but with only the RSC passing cluster correction; the red contour signifies the mask used for RSC, derived from NeuroSynth. The middle columns display the average confusion matrix for this region, again with percentages of predicted distances against true distances. The right columns display the average classification accuracy (\pm SE) for each interval, for display purposes only; the dashed line represents chance performance. All significant clusters at height p < .001 and cluster p < .05 FWE corrected.

relates to the fidelity with which participants reproduce intervals. Indeed, given that participants exhibited differences in the degree of central tendency between tasks, it is possible that decoding was in fact driven by this difference (see Hayashi, van der Zwaag, Bueti, & Kanai, 2018, for a similar analysis). To address this, we correlated decoding accuracy within the SMA and RSC with the degree of central tendency between participants. However, no significant correlations were observed for either time (r = -.29, p = .27) or distance (r = .02, p = .93), suggesting that decoding accuracy was not driven by the degree to which participants exhibited central tendency.

Multivariate Timing Differs between Estimation and Reproduction

To further examine decoding performance, we next examined accuracy in the estimation phase, when participants walked for an unknown distance or time. Here, no significant regions were detected for the distance estimation phase. However, the time estimation phase exhibited significant accuracy decoding in several regions, including the SMA, precentral gyrus, and right inferior frontal gyrus

(Figure 4). As a comparison with the reproduction phase, we extracted the beta values from the SMA region for estimation and reproduction phases and compared them. We conducted this analysis to differentiate possible responses between encoding and reproduction. When examining the beta values for each interval, across estimation and reproduction phases, we observed that beta values were flat while estimating progressively longer durations (Hayashi et al., 2018), suggesting that the overall pattern of activation across voxels drove decoding performance. However, during the reproduction phase, we instead observed a linear increase in the modeled BOLD response in the SMA (Figure 4). A repeated-measures ANOVA confirmed these observations, with a significant effect of Phase (estimation vs. reproduction, F(1, 15) = 15.896, p = .001, $\eta^2 = .217$) and Phase × Interval interaction, $F(6, 90) = 3.06, p = .009, \eta 2 = .043$. As such, both patterns were observed in the SMA at distinct phases, suggesting the SMA operates in two modes when timing virtual movement, a point we turn to in the discussion. We further note that this analysis avoids circularity, or "double-dipping," as the analysis conducted on the beta values (repeatedmeasures ANOVA) is independent of the type of analysis

Table 4. Multivariate Decoding Results

Location	Cluster Size	t Value	\mathcal{X}	\mathcal{Y}	z
Time Decoding (Estimation)					
R SMA	404	7.263	11	-2	50
R superior medial gyrus		5.616	8	33	45
R superior parietal lobe	460	7.008	23	-60	65
R Inferior parietal lobe		3.869	43	-55	55
R precuneus		3.870	3	-55	68
L superior occipital gyrus	340	6.517	-25	-80	45
L precuneus		4.294	-5	-47	55
L middle frontal gyrus	385	6.039	-37	8	40
L middle frontal gyrus		5.953	-25	-7	53
Time Decoding (Reproduction)					
L precentral gyrus	537	5.795	-40	-7	50
L postcentral gyrus		4.448	-50	-15	33
L IFG (p. opercularis)		4.177	-47	11	28
L SMA	205	5.046	-5	18	60
R IFG (p. opercularis)	214	4.581	48	8	35
Distance Decoding (Reproducti	on)				
R precuneus (RSC)*	22	5.401	11	-52	13
Cerebellar vermis (4/5)	15	5.263	6	-60	-15
L caudate	100	4.737	-15	18	20
L cerebellum (VIII)	13	4.176	-37	-50	-50
Cross-classification (Estimation))				
R middle occipital gyrus	354	9.925	33	-70	5
R calcarine gyrus		7.074	21	-87	10
R supramarginal gyrus	113	9.808	48	-37	43

that drove selection of those voxels (multivariate classification; Kriegeskorte, Simmons, Bellgowan, & Baker, 2009). Finally, we again correlated decoding accuracy with central tendency, but also observed no significant correlation (r=.19, p=.464), suggesting these effects also were not driven by regression to the mean in behavioral responses.

Cross-classification Decoding

As a final comparison, we tested for abstract representations of magnitude. To accomplish this, we took a cross-

classification approach (Kaplan, Man, & Greening, 2015), in which a classifier was trained on activation patterns from the seven intervals in one dimension (e.g., time) and tested on patterns from intervals in the other dimension (e.g., distance). Previous work has demonstrated that the right inferior parietal lobe may serve as an abstract representation of magnitude, such that this region processes the general size of continuous stimulus representations (Bueti & Walsh, 2009). We examined classification accuracy bidirectionally, such that significant performance represented regions that could crossclassify above chance in either direction. Here, two

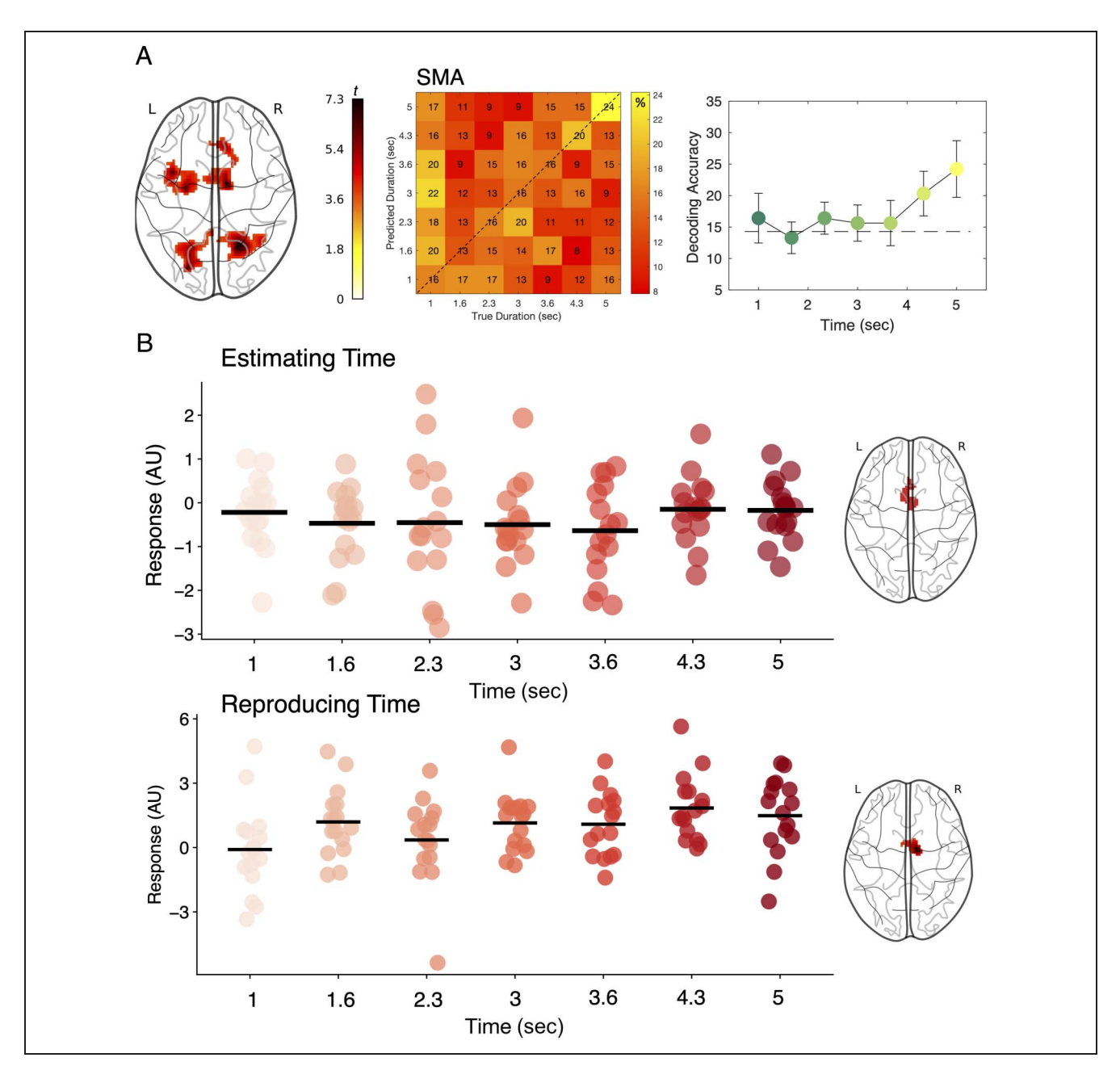


Figure 4. Comparison of time decoding in the SMA reveals different coding properties for estimation and reproduction. (A) Significant clusters for decoding time walked during the estimation phase, revealing activity in SMA, precentral gyrus, and bilateral superior parietal cortex. The middle column displays the average confusion matrix for the SMA region, displaying percentage of predicted duration against true duration; the right column displays the average classification accuracy (\pm SE) for each interval relative to chance (dashed line), for display purposes only. (B) Beta values within the SMA region (averaged across regions from right brain images) for the time estimation and reproduction phases; black bars indicate the mean. For the estimation phase, beta values exhibited no difference across presented times. However, for the reproduction phase, SMA beta values increased linearly with increasing duration. All clusters significant at height p < .001, clusters p < .001 FWE corrected.

regions were observed that survived significance testing: the right supramarginal gyrus (rSMG) and a cluster within the right middle occipital gyrus (Figure 5, Table 4). To further determine the nature of the occipital cluster, we compared this region to a recently released probabilistic functional atlas of visual cortex (Rosenke, van Hoof, van

den Hurk, Grill-Spector, & Goebel, 2021). Here, we observed that the occipital cluster most closely overlapped with the probable location of the occipital place area (OPA), a region that activates in response to visual scenes, with potential navigation functions (Epstein, Patai, Julian, & Spiers, 2017).

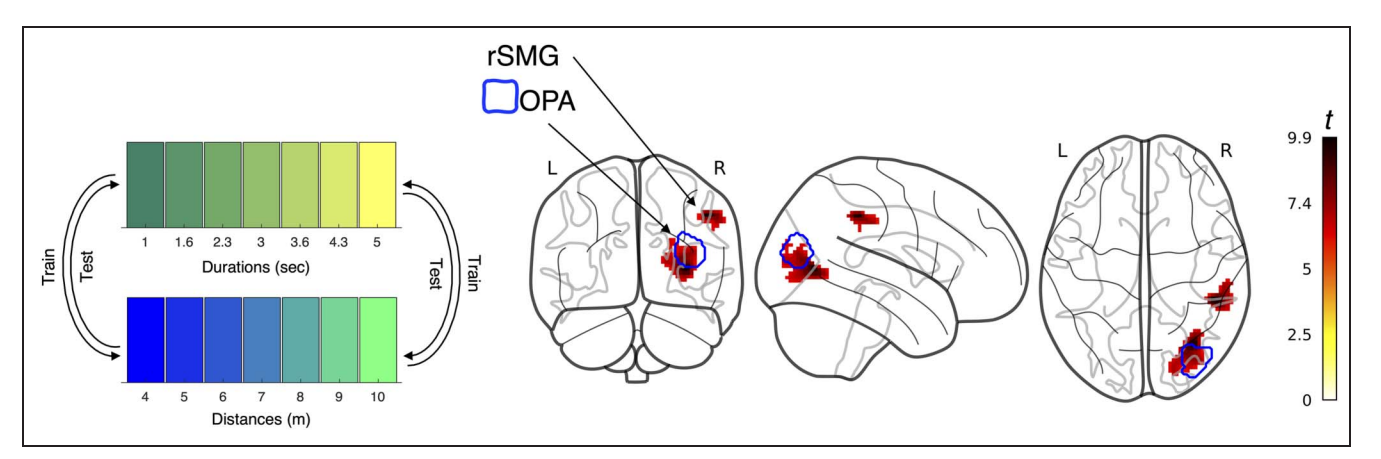


Figure 5. Results of cross-classification decoding, demonstrating dimension-nonspecific representations of time and distance. On the left, classifiers were separately trained one dimension (e.g., time) and then tested on the alternate dimension (e.g., distance). On the right, two significant clusters of activation were observed within the rSMG and lateral occipital cortex. The blue contour represents a probable mask of the OPA, derived from Rosenke et al. (2021).

DISCUSSION

Behaviorally, we observed central tendency for both time and space, similar to other studies using the same paradigm; however, this effect was significantly larger for time than for space and was correlated between dimensions. This suggests that there may be a common mechanism for reproducing different magnitudes regardless of dimension (i.e., time, space, size). On the other hand, variability of reproductions showed no difference between time and distance; therefore, participants were equally consistent when reproducing either dimension.

Similar to previous fMRI findings (Wiener et al., 2016), during distance reproduction, a broad network of brain regions were activated including the basal ganglia, cerebellum, ACC, right pFC, parietal and occipital regions, and the hippocampus. In addition, during time reproduction, similar networks were activated excluding the hippocampus. When contrasting the activation during reproduction between both dimensions, we found a dissociation across the central sulcus in that distance activated a cluster of posterior regions extending from the middle occipital gyri to the inferior parietal lobes and from the thalamus to the cerebellum and bilateral hippocampus, whereas time solely activated the SMA, bilaterally. This suggests that the brain coordinates movements for distance and time between rostral and caudal regions. We additionally found that time and distance can be decoded during reproduction; specifically, the region that could most accurately decode time was observed in the SMA, whereas the region that could most accurately decode space was observed in the RSC.

We additionally examined decoding performance for the estimation phase of the task; in this case, no specific regions could accurately decode the distance estimation phase; however, several regions could decode the time estimation phase including the SMA, precentral gyrus, and right inferior frontal gyrus. Given that the SMA was able to decode time in both estimation and reproduction, we further examined this region by extracting beta values for both phases and compared them. We found that when participants were estimating longer durations, the beta values remained flat (Hayashi et al., 2018); however, in the reproduction phase, we observed a linear increase in the BOLD response in the SMA. This finding suggests that the SMA operates in different modes when timing virtual movement depending on the phase (i.e., estimation vs. reproduction). We further emphasize that the flat responses in the estimation phase suggests that decoding accuracy was not driven by longer time intervals leading to larger responses. Rather, the estimation phase finding suggests the pattern of activation drives decoding performance, which may be the result of independent channels associated with distinct intervals (Jazayeri & Shadlen, 2015), or a tuning mechanism for specific intervals (Protopapa et al., 2019); further work will be necessary to disentangle these possibilities. In contrast, the reproduction finding is in line with work that suggests that the SMA exhibits activation patterns consistent with a temporal accumulator, similar to properties of the contingent negative variation (CNV) during EEG, in which activity increases with elapsing intervals (Mita, Mushiake, Shima, Matsuzaka, & Tanji, 2009). We further note that the linear activation pattern of the SMA is timelocked to the onset of the reproduction phase. This pattern shows a striking similarity to that observed recently in EEG data from this same task (Robinson & Wiener, 2021); larger CNV amplitude responses were observed corresponding to longer intended or planned intervals. Considering putative correspondence between the CNV and SMA activity (Nagai et al., 2004), we suggest both reflect the same mechanism. More specifically, we suggest this amplitude change reflects a preplanning signal for reproducing time intervals, as has been observed previously in non-human primates (Jazayeri & Shadlen, 2015).

Last, we wanted to further corroborate previous work suggesting that the right inferior parietal lobe is important

for the representation of different magnitudes regardless of dimension using a cross-classification approach (Bueti & Walsh, 2009). We note that two regions were found to cross-classify above chance in either direction, the rSMG located in the right inferior parietal lobe as well as the right middle occipital gyrus. The rSMG finding suggests that the right inferior parietal lobe does represent general magnitudes. We found that the occipital cluster appeared to overlap with the probable location of the OPA, which activates when viewing visual scenes and has been suggested to be responsible for potential navigation functions (Rosenke et al., 2021; Epstein et al., 2017). This suggests that the OPA decoding accuracy related to the visual experience of walking distances.

Taken together, these findings suggest that reproducing time and distance activate a similar corticalsubcortical network of regions divided between anterior and posterior regions, respectively, and that the duration and distance walking can be accurately decoded from activation in the SMA and RSC, respectively. In addition, the findings support a potential dimension-nonspecific decoder in the rSMG and occipital cortex located approximately at the OPA, suggesting this area of the brain encodes both distance and duration traveled from a starting location in the environment. We note that crossclassification approaches, as opposed to standard classification, provide a unique window into the association between brain activity and stimulus responses (Kaplan et al., 2015). Indeed, although the rSMG and parts of the occipital cortex were also active in both univariate contrasts within each dimension, we note that they were absent in the within-dimension classification analyses. One possible reason for this discrepancy is that the cross-classification analysis was more sensitive to patterns that distinguish across dimensions, rather than within a given dimension (see Kaplan et al., 2015, for a discussion of this issue). One method to tease the roles of these regions apart would be to administer brain stimulation to distinct regions implicated in both within- and cross-classification analyses and observe resultant changes in performance.

Finally, the findings point to a simple circuit model describing how time and distance measurements interact (Figure 6). Specifically, duration and distance estimates appear to be encoded via separate channels, each of which may be manipulated by the amount of attention focused on them; these estimates then interact in memory, before judgments are being made at a planning stage. Neurally, the RSC, SMA, IPL, and pFC all appear to be active, but in different ways. Specifically, the RSC and SMA both appear to encode and store intervals of distance and duration, respectively. These intervals are then passed to the pFC as vectors for movement (Harootonian, Wilson, Hejtmánek, Ziskin, & Ekstrom, 2020; Leek & Johnston, 2009) that include both the distance (V_d) and duration (V_t) of the required action. Furthermore, we suggest the IPL encodes the covariance of distance and time as a supramodal signal for magnitude.

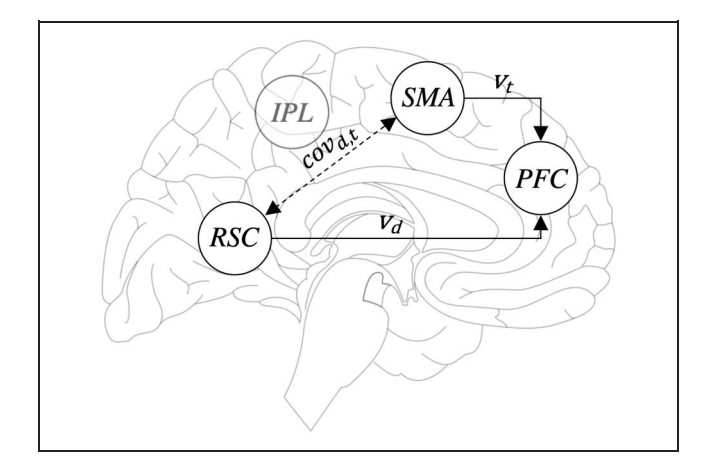


Figure 6. Diagram of a simple model of results. The SMA and RSC serve as reference points for time and distance, respectively. Accordingly, each region encodes a vector (v), for time (v_t) in the SMA, and distance (v_d) in the RSC while navigating from an origin point. These vectors are in turn processed by prefrontal regions during path integration. In addition, the covariance between distance and time (cov_{d_t}, t) is implicitly encoded in the IPL, which shares connections with each of these regions.

We suggest this circuit model provides a parsimonious explanation for the roles of the RSC and the SMA in the processing of time and space. For space, the RSC has been associated with path integration, transitions between viewpoints, and landmark recognition (Chrastil, 2018). In particular, the RSC may serve as an anchor for movements in the environment, such that an observer can keep track of their point of origin (Marchette, Vass, Ryan, & Epstein, 2014). For time, the SMA has been associated with a temporal accumulation process, but also has shown involvement in tracking relative differences between experienced time and remembered intervals (Mendoza, Méndez, Pérez, Prado, & Merchant, 2018). We suggest that this latter comparison process is similar to placing an anchor in time, that is, tracking how much time has elapsed from a given event, a necessary component of navigating through the environment. Both processes may be deployed in the service of action, for choosing between different paths to travel to achieve a particular goal.

Regarding limitations of the present study, we note limitations in our sample size and so stress caution in interpreting our findings without further investigation. In addition, because of differences between trialwise and blockwise performance on this task, where the to-beattended dimension changes, it is possible that participants employed different strategies for completing each task (Robinson & Wiener, 2021).

Overall, our findings demonstrate that time and distance can be both separately, and conjointly, decoded from brain activation patterns in distinct parts of the brain. These findings suggest that the brain holds separate metrics for each dimension, while also tracking a general magnitude for travel. Future studies will be necessary to determine how time and space metrics are combined

downstream and how disruptions in one dimension may impact the processing of the other.

Corresponding author: Martin Wiener, Department of Psychology, George Mason University, 4400 University Drive, Fairfax, VA 22030, or via e-mail: mwiener@gmu.edu.

Data Availability Statement

All behavioral data is available at Neurovalut.org: https://identifiers.org/neurovault.collection:16113

Author Contributions

Keri Gladhill: Data curation; Investigation; Methodology; Project administration. Eva Marie Robinson: Conceptualization; Investigation; Methodology; Software. Candice Stanfield-Wiswell: Data curation; Investigation. Farah Bader: Data curation; Investigation; Project administration. Martin Wiener: Data curation; Investigation; Methodology; Project administration.

Diversity in Citation Practices

Retrospective analysis of the citations in every article published in this journal from 2010 to 2021 reveals a persistent pattern of gender imbalance: Although the proportions of authorship teams (categorized by estimated gender identification of first author/last author) publishing in the *Journal of Cognitive Neuroscience* (*JoCN*) during this period were M(an)/M = .407, W(oman)/M = .32, M/W = .115, and W/W = .159, the comparable proportions for the articles that these authorship teams cited were M/M = .549, W/M = .257, M/W = .109, and W/W = .085 (Postle and Fulvio, *JoCN*, 34:1, pp. 1–3). Consequently, *JoCN* encourages all authors to consider gender balance explicitly when selecting which articles to cite and gives them the opportunity to report their article's gender citation balance.

REFERENCES

- Bansal, A., Weech, S., & Barnett-Cowan, M. (2019). Movement-contingent time flow in virtual reality causes temporal recalibration. *Scientific Reports*, *9*, 4378. https://doi.org/10.1038/s41598-019-40870-6, PubMed: 30867525
- Bueti, D., & Walsh, V. (2009). The parietal cortex and the representation of time, space, number and other magnitudes. *Philosophical Transactions of the Royal Society of London, Series B: Biological Sciences*, 364, 1831–1840. https://doi.org/10.1098/rstb.2009.0028, PubMed: 19487186
- Cai, Z. G., & Connell, L. (2016). On magnitudes in memory: An internal clock account of spacetime interaction. *Acta Psychologica*, *168*, 1–11. https://doi.org/10.1016/j.actpsy.2016.04.003, PubMed: 27116395
- Chrastil, E. R. (2018). Heterogeneity in human retrosplenial cortex: A review of function and connectivity. *Behavioral Neuroscience*, *132*, 317–338. https://doi.org/10.1037/bne0000261, PubMed: 30160506

- Cona, G., & Scarpazza, C. (2019). Where is the where in the brain? A meta-analysis of neuroimaging studies on spatial cognition. *Human Brain Mapping*, 40, 1867–1886. https://doi.org/10.1002/hbm.24496, PubMed: 30600568
- Cona, G., Wiener, M., & Scarpazza, C. (2021). From ATOM to GradiATOM: Cortical gradients support time and space processing as revealed by a meta-analysis of neuroimaging studies. *Neuroimage*, 224, 117407. https://doi.org/10.1016/j .neuroimage.2020.117407. PubMed: 32992001
- Coull, J. T., Charras, P., Donadieu, M., Droit-Volet, S., & Vidal, F. (2015). SMA selectively codes the active accumulation of temporal, not spatial, magnitude. *Journal of Cognitive Neuroscience*, 27, 2281–2298. https://doi.org/10.1162/jocn_a 00854, PubMed: 26226079
- Deuker, L., Bellmund, J. L., Navarro, S. T., & Doeller, C. F. (2016). An event map of memory space in the hippocampus. *eLife*, *5*, e16534. https://doi.org/10.7554/eLife.16534, PubMed: 27710766
- Eisler, H. (1976). Experiments on subjective duration 1968-1975: A collection of power function exponents. *Psychological Bulletin*, *83*, 1154–1171. https://doi.org/10.1037/0033-2909.83 .6.1154, PubMed: 996212
- Epstein, R. A., Patai, E. Z., Julian, J. B., & Spiers, H. J. (2017). The cognitive map in humans: Spatial navigation and beyond. *Nature Neuroscience*, *20*, 1504–1513. https://doi.org/10.1038/nn.4656, PubMed: 29073650
- Gauthier, B., & van Wassenhove, V. (2016). Time is not space: Core computations and domain-specific networks for mental travels. *Journal of Neuroscience*, *36*, 11891–11903. https://doi.org/10.1523/JNEUROSCI.1400-16.2016, PubMed: 27881776
- Harootonian, S. K., Wilson, R. C., Hejtmánek, L., Ziskin, E. M., & Ekstrom, A. D. (2020). Path integration in large-scale space and with novel geometries: Comparing vector addition and encoding-error models. *PLoS Computational Biology*, 16, e1007489. https://doi.org/10.1371/journal.pcbi.1007489, PubMed: 32379824
- Hayashi, M. J., van der Zwaag, W., Bueti, D., & Kanai, R. (2018). Representations of time in human frontoparietal cortex. *Communications Biology*, 1, 233. https://doi.org/10.1038/s42003-018-0243-z, PubMed: 30588512
- Hebart, M. N., Görgen, K., & Haynes, J.-D. (2015). The decoding toolbox (TDT): A versatile software package for multivariate analyses of functional imaging data. *Frontiers in Neuroinformatics*, 8, 88. https://doi.org/10.3389/fninf.2014 .00088, PubMed: 25610393
- Jazayeri, M., & Shadlen, M. N. (2010). Temporal context calibrates interval timing. *Nature Neuroscience*, 13, 1020–1026. https://doi.org/10.1038/nn.2590, PubMed: 20581842
- Jazayeri, M., & Shadlen, M. N. (2015). A neural mechanism for sensing and reproducing a time interval. *Current Biology*, 25, 2599–2609. https://doi.org/10.1016/j.cub.2015.08.038, PubMed: 26455307
- Kaplan, J. T., Man, K., & Greening, S. G. (2015). Multivariate cross-classification: Applying machine learning techniques to characterize abstraction in neural representations. *Frontiers* in *Human Neuroscience*, 9, 151. https://doi.org/10.3389 /fnhum.2015.00151, PubMed: 25859202
- Kim, M., & Maguire, E. A. (2018). Hippocampus retrosplenial and parahippocampal cortices encode multicompartment 3D space in a hierarchical manner. *Cerebral Cortex*, 28, 1898–1909. https://doi.org/10.1093/cercor/bhy054, PubMed: 29554231
- Kriegeskorte, N., Simmons, W. K., Bellgowan, P. S., & Baker, C. I. (2009). Circular analysis in systems neuroscience: The dangers of double dipping. *Nature Neuroscience*, 12, 535–540. https://doi.org/10.1038/nn.2303, PubMed: 19396166

- Leek, E. C., & Johnston, S. J. (2009). Functional specialization in the supplementary motor complex. *Nature Reviews Neuroscience*, 10, 78. https://doi.org/10.1038/nrn2478-c1, PubMed: 19096371
- Marchette, S. A., Vass, L. K., Ryan, J., & Epstein, R. A. (2014). Anchoring the neural compass: Coding of local spatial reference frames in human medial parietal lobe. *Nature Neuroscience*, *17*, 1598–1606. https://doi.org/10.1038/nn.3834, PubMed: 25282616
- Marcos, E., & Genovesio, A. (2017). Interference between space and time estimations: From behavior to neurons. *Frontiers in Neuroscience*, 11, 631. https://doi.org/10.3389/fnins.2017 .00631, PubMed: 29209159
- Martin, B., Wiener, M., & van Wassenhove, V. (2017). A Bayesian perspective on accumulation in the magnitude system. *Scientific Reports*, 7, 630. https://doi.org/10.1038/s41598-017-00680-0, PubMed: 28377631
- Mendoza, G., Méndez, J. C., Pérez, O., Prado, L., & Merchant, H. (2018). Neural basis for categorical boundaries in the primate pre-SMA during relative categorization of time intervals. Nature Communications, 9, 1098. https://doi.org/10.1038/s41467-018-03482-8, PubMed: 29545587
- Mita, A., Mushiake, H., Shima, K., Matsuzaka, Y., & Tanji, J. (2009). Interval time coding by neurons in the presupplementary and supplementary motor areas. *Nature Neuroscience*, *12*, 502–507. https://doi.org/10.1038/nn.2272, PubMed: 19252498
- Nagai, Y., Critchley, H. D., Featherstone, E., Fenwick, P. B. C., Trimble, M. R., & Dolan, R. J. (2004). Brain activity relating to the contingent negative variation: An fMRI investigation. *Neuroimage*, 21, 1232–1241. https://doi.org/10.1016/j .neuroimage.2003.10.036, PubMed: 15050551
- Peer, M., Ron, Y., Monsa, R., & Arzy, S. (2019). Processing of different spatial scales in the human brain. *eLife*, 8, e47492. https://doi.org/10.7554/eLife.47492, PubMed: 31502539
- Petzschner, F. H., & Glasauer, S. (2011). Iterative Bayesian estimation as an explanation for range and regression effects: A study on human path integration. *Journal of Neuroscience*, *31*, 17220–17229. https://doi.org/10.1523/JNEUROSCI.2028-11.2011, PubMed: 22114288
- Pfeuty, M., Ragot, R., & Pouthas, V. (2003). When time is up: CNV time course differentiates the roles of the hemispheres in the discrimination of short tone durations. *Experimental Brain Research*, *151*, 372–379. https://doi.org/10.1007/s00221-003-1505-6, PubMed: 12819842
- Protopapa, F., Hayashi, M. J., Kulashekhar, S., van der Zwaag, W., Battistella, G., Murray, M. M., et al. (2019). Chronotopic maps in human supplementary motor area. *PLoS Biology*,

- 17, e3000026. https://doi.org/10.1371/journal.pbio.3000026, PubMed: 30897088
- Rattat, A. C., & Droit-Volet, S. (2012). What is the best and easiest method of preventing counting in different temporal tasks? *Behavior Research Methods*, 44, 67–80. https://doi.org/10.3758/s13428-011-0135-3, PubMed: 21789731
- Riemer, M. (2015). Psychophysics and the anisotropy of time. *Consciousness and Cognition*, *38*, 191–197. https://doi.org/10.1016/j.concog.2015.06.007, PubMed: 26121957
- Riemer, M., Achtzehn, J., Kuehn, E., & Wolbers, T. (2022). Cross-dimensional interference between time and distance during spatial navigation is mediated by speed representations in intraparietal sulcus and area hMT. *Neuroimage*, 257, 119336. https://doi.org/10.1016/j.neuroimage.2022.119336, PubMed: 35643266
- Riemer, M., & Wolbers, T. (2020). Negative errors in time reproduction tasks. *Psychological Research*, 84, 168–176. https://doi.org/10.1007/s00426-018-0994-7, PubMed: 29460144
- Robinson, E., Michaelis, K., Thompson, J. C., & Wiener, M. (2019). Temporal and spatial discounting are distinct in humans. *Cognition*, 190, 212–220. https://doi.org/10.1016/j .cognition.2019.04.030, PubMed: 31121404
- Robinson, E. M., & Wiener, M. (2021). Dissociable neural indices for time and space estimates during virtual distance reproduction. *Neuroimage*, *226*, 117607. https://doi.org/10.1016/j.neuroimage.2020.117607, PubMed: 33290808
- Rosenke, M., van Hoof, R., van den Hurk, J., Grill-Spector, K., & Goebel, R. (2021). A probabilistic functional atlas of human occipito-temporal visual cortex. *Cerebral Cortex*, *31*, 603–619. https://doi.org/10.1093/cercor/bhaa246, PubMed: 32968767
- Ruthotto, L., Kugel, H., Olesch, J., Fischer, B., Modersitzki, J., Burger, M., et al. (2012). Diffeomorphic susceptibility artifact correction of diffusion-weighted magnetic resonance images. *Physics in Medicine and Biology*, *57*, 5715–5731. https://doi.org/10.1088/0031-9155/57/18/5715, PubMed: 22941943
- Thurley, K., & Schild, U. (2018). Time and distance estimation in children using an egocentric navigation task. *Scientific Reports*, *8*, 18001. https://doi.org/10.1038/s41598-018-36234-1, PubMed: 30573744
- Wiener, M., Michaelis, K., & Thompson, J. C. (2016). Functional correlates of likelihood and prior representations in a virtual distance task. *Human Brain Mapping*, 37, 3172–3187. https://doi.org/10.1002/hbm.23232, PubMed: 27167875
- Wiener, M., Turkeltaub, P., & Coslett, H. B. (2010). The image of time: A voxel-wise meta-analysis. *Neuroimage*, 49, 1728–1740. https://doi.org/10.1016/j.neuroimage.2009.09 .064, PubMed: 19800975